

Plasticity of hexagonal systems: Split slip modes and inverse Peierls relation in α -Ti

Piotr Kwaśniak, Piotr Śpiewak, Halina Garbacz, and Krzysztof J. Kurzydłowski

Materials Design Division, Faculty of Materials Science and Engineering, Warsaw University of Technology, Włocławska 141, 02-507 Warsaw, Poland

(Received 24 September 2013; revised manuscript received 6 March 2014; published 11 April 2014)

The plasticity of hexagonal titanium is reexamined based on the split slip modes phenomenon, revealing the existence of subslip modes in prismatic and pyramidal hcp slip systems. The energetics of dislocation emission and motions were described using all-dimension relaxed atomic models of crystal slip, calculated with density functional theory. The proposed computational methodology is based on the generalized stacking fault energy concept and respects all elastic effects arising within dislocation nucleation. As a result, improved accuracy has been obtained with regard to ductility prediction and a breach has been discovered in the fundamental Peierls-Nabarro rule. This approach is essential for the Rice and Peierls-Nabarro models and can be used as an effective tool for ductility predictions when designing new hexagonal alloys.

DOI: [10.1103/PhysRevB.89.144105](https://doi.org/10.1103/PhysRevB.89.144105)

PACS number(s): 62.20.fk, 61.50.Ah, 61.72.Nn, 62.20.fq

I. INTRODUCTION

Intense research in green technologies is focusing on reducing energy consumption in all transport sectors, providing incentives for designing new light, strong materials. Taking into account these two parameters, it is clear that Ti and Mg, which have the highest strength-to-density ratios, are potentially prime elements when considering new constructional alloys. Of the various key requirements, ductility seems to be crucial from the production and application points of view. As a consequence, there has been much interest shown in developing plastic deformation theory and practical methods that allow one to predict the brittle/ductile behavior of materials. Complex and universal models are the current challenge in the field of alloy design.

There are a number of methods for estimating the ductility of materials. The most important ones include the analysis of the electronic structure and directionality/type of chemical bonds [1] and values of elastic constants such as the Poisson ratio and Pugh's criterion [2]. While these methods are common, they do not reflect the physics of plastic deformation such as dislocation emission and motion. A direct approach to this problem can be found in the Peierls-Nabarro (P-N) model [3,4], which was the first meaningful assessment of lattice resistance during dislocation motion. The next key achievement was the concept of the generalized stacking fault energy surface (γ surface) introduced by Christian and Vítek [5]. The γ surface is the interplanar potential energy for sliding one-half of a rigid crystal over the other half along the glide plane through an arbitrary vector δ . The importance of the γ surface lies in periodic distribution of restoring stresses,

$$F(\delta) = -\nabla[\gamma(\delta)], \quad (1)$$

which determine lattice resistance during dislocation nucleation, while its physical meaning is similar to Peierls stress (critical stress needed for translation of rigid dislocations at zero temperature) in the P-N model [3]. Both quantities impede deformation by slip of the dislocations. The adoption of the γ surface facilitated rapid development of the P-N model and the dislocation properties [6–9], with the conclusion that Peierls stress can be estimated directly from the γ surface [7]. Another concept of the ductility of materials in terms

of dislocation emission was postulated by Rice and Thomson [10]. They proposed that the onset of ductile behavior occurred when the spontaneous emission of dislocations at the crack tip became feasible. Further, Rice showed that the unstable stacking fault energy, γ_{us} (maximum of the γ surface), is a measure of the energy barrier for dislocation nucleation [11]. The above achievements, although incredibly valuable for deformation by dislocation emission/motion, do not cover the twinning phenomenon. This gap was filled by Tadmor and Hai [12], who reported that critical stresses needed to generate leading, trailing, and twinning partial dislocations can be expressed using γ_{us} , γ_{st} (γ minimum at path for partial dislocation), and γ_{ut} (γ maximum for twinning partial dislocation). This allowed them to form the new material parameter called *twinning tendency*. An excellent summary of the presented notions is the *disembrittlement* (D) parameter introduced by Waghmare *et al.* [13], who concluded that γ_{us} is fundamental for all current models and the increase/decrease of $D = \text{free surface energy}/\gamma_{us}$ leads to the increase/decrease of ductility.

The main inaccuracy of the approaches listed above is the fact that they are based on the γ surface, which is a nonphysical projection of crystal slip. Dislocation emission and motion incorporate two energy components: (1) initial elastic deformation and (2) breaking of atomic bonds. While the second term can be assessed by the γ surface, the contribution of elastic deformation is absent from the rigid γ model.

In this paper, we propose a computational approach containing an all-dimension relaxation procedure that overcomes the “rigid γ ” problem and radically improves the *ab initio* predictions of crystal slip. Our method has been used to inform a comprehensive study of α -Ti plasticity—multiple glide plane system. We also show the separation of slip modes effect occurring in hexagonal structures, which is fundamental to the physics of plastic deformation.

II. SEPARATION OF SLIP MODES IN HEXAGONAL Ti

The plastic deformation theory establishes that nucleation and the motion of dislocations are possible for certain directions and planes called slip systems. The group of active

slip systems can be obtained from the original P-N model [14,15], which allows one to assess the critical stress σ_P needed to move rigid dislocation:

$$\sigma_P = \frac{2\mu}{1-\nu} \exp \left[-\frac{2\pi d}{b(1-\nu)} \right], \quad (2)$$

where μ , ν are elastic constants and b , d are Burgers vector and interplanar spacing, respectively. Although Eq. (2) assumes a sinusoidal form of the restoring stress (which is not always correct), it reproduces well the strong correlations between Burgers vector, interplanar distance, and Peierls stress σ_P —increased interplanar distance and decreased length of the Burgers vectors lead to a reduction of Peierls stress. The dependence presented in Eq. (2) is called the Peierls relation and is widely used in the physics of plastic deformation. Based on this knowledge, most of the slip modes in typical crystal lattices have been identified and described [14,16].

Plastic deformation in α -Ti can be realized by four types of slip systems on three glide planes [17]: $\langle 11\bar{2}0 \rangle$ (0001) - $\langle a \rangle$ on the basal plane, $\langle 11\bar{2}0 \rangle$ $\{10\bar{1}0\}$ - $\langle a \rangle$ on the prismatic plane, $\langle 11\bar{2}0 \rangle$ $\{10\bar{1}1\}$ - $\langle a \rangle$ on the pyramidal plane, $\langle 11\bar{2}3 \rangle$ $\{10\bar{1}1\}$ - $\langle c+a \rangle$ on the pyramidal plane, and a fifth deformation mode, namely, twinning. It is reported that the critical resolved shear stress (CRSS) for systems with $\langle a \rangle$ Burgers vector is relatively similar and the $\langle c+a \rangle$ $\{10\bar{1}1\}$ system exhibits a distinctly higher CRSS value [17,18]. Moreover, it should be noted that all modes are sensitive to the presence of dopants and alloying elements, which can suppress or enhance individual systems differently [18,19]. Various reactions of slip systems to the presence of alloying elements make hexagonal structures problematic during the alloy design process, and, for correct ductility prediction, all systems have to be taken into account.

Figure 1(a) shows a set of slip systems in fcc, bcc, and hcp crystal structure—which are the most common for metals. According to the current definition of slip modes and the Peierls rule, nucleation and motion of dislocation should be fully described using only indexes of directions and planes. Considering the slip systems in both cubic fcc and bcc crystal lattices, it is evident that glide planes exhibit constant interplanar distance in particular modes, similarly to the $\langle a \rangle$ basal mode in the hcp structure. However, an entirely different situation can be observed for hcp prismatic and pyramidal planes. In these cases, two types of interplanar distance exist that differ significantly in size. The prismatic and pyramidal planes also have a fourfold stacking sequence, ABCDABCD..., which is presented in Fig. 1(c). Those structural features lead to a key fact: in hcp systems, two types of each prismatic and pyramidal slip modes exist which have the same type of slip planes and Burgers vector plus various interplanar spacing. In Fig. 1(c), the dashed lines denote possible glide planes for all prismatic and pyramidal modes, and I, II symbols represent the Burgers vectors. Although the vectors are equivalent (same direction and length for individual systems), it is clear that the interplanar distance is unequal and slip may be performed in various ways along modes I or II. As an example, for $\langle a \rangle$ prismatic systems, red atoms have differently located neighbors than green atoms (red/green atoms slide over green/blue ones in types I and II, respectively), which should also result in various γ shapes and σ_P for both modes. Concluding the observations above,

the standard definition of slip systems fails in hcp prismatic and pyramidal planes since it does not reveal the existence of separate modes (I and II) and, for a precise description of these systems, information about interplanar distance must be added.

Despite numerous works devoted to the plasticity of hexagonal structures, including recent experimental [17] and theoretical [20] investigations, the dual nature of pyramidal and prism planes has not been noticed. It should be emphasized that various interplanar distances between atomic planes with the same indexes cannot occur in face- or body-centered-cubic lattices due to their higher structural symmetry (Fig. 1). The existence of additional parameters (the interplanar distance), which need to be taken into account for a full description of slip modes, begs the fundamental question: Which system is easier/active? The answer should be found in the Peierls rule derived from the original P-N model. Nevertheless, the P-N concept does not give any special information about structures in which slip planes exhibit double types of interplanar distance. In order to surmount the above uncertainties and to establish active slip systems in α -Ti, γ calculations have been performed for all types of slip modes. Regarding the various interplanar distance, the list of possible slip systems can be written anew [Fig. 1(c)]: $\langle a \rangle$ basal, $\langle a \rangle$ prismatic I, $\langle a \rangle$ prismatic II, $\langle a \rangle$ pyramidal I, $\langle a \rangle$ pyramidal II, $\langle c+a \rangle$ pyramidal I, and $\langle c+a \rangle$ pyramidal II, where I or II denote large or small interplanar spacing, respectively. Additionally, the modes marked with symbols I or II are called, here, *the split modes*.

III. METHOD

The *ab initio* calculations of γ curves were done in two ways. First, conventional (all atoms are relaxed only in directions perpendicular to the glide planes and displacements of the crystal half part along the direct slip path are constants) computations of direct crystal slips for all seven slip modes were performed using density functional theory (DFT) implemented in the Vienna *Ab initio* Simulation Package (VASP) code [21,22], with the projector augmented wave (PAW) method for core-valence electron interaction [23]. To estimate the exchange and correlation energy, the Perdew-Burke-Ernzerhof (PBE) [24] functional was adopted. The Fermi smearing of the electronic occupancy with 0.2 eV and plane-wave cutoff energy of 425 eV were used. The Brillouin zone was sampled in accordance with the Monkhorst-Pack scheme [25]. A large number of preliminary γ curve calculations were performed to establish the correct size of the atomic structures used in the computations. Finally, 18 atomic layer models (4 atoms in each plane) with 8, 12, and 10 Å of free space, respectively, for basal ($5 \times 5 \times 1$ k -points mesh), prism ($3 \times 5 \times 3$ k points), and pyramidal ($3 \times 5 \times 3$ k points) slip modes were chosen for calculations [Fig. 1(c)]. Increasing the size of the atomic planes did not lead to better accuracy of the γ results since all Burgers vectors and elastic displacements of the atoms were much smaller than the dimensions of the atomic models. At this point, an important issue must be highlighted: the γ model does not contain a dislocation line and, consequently, the increased size of the supercell is not needed—all considered effects are fully periodic in each unit cell. Similarly, the number of atomic

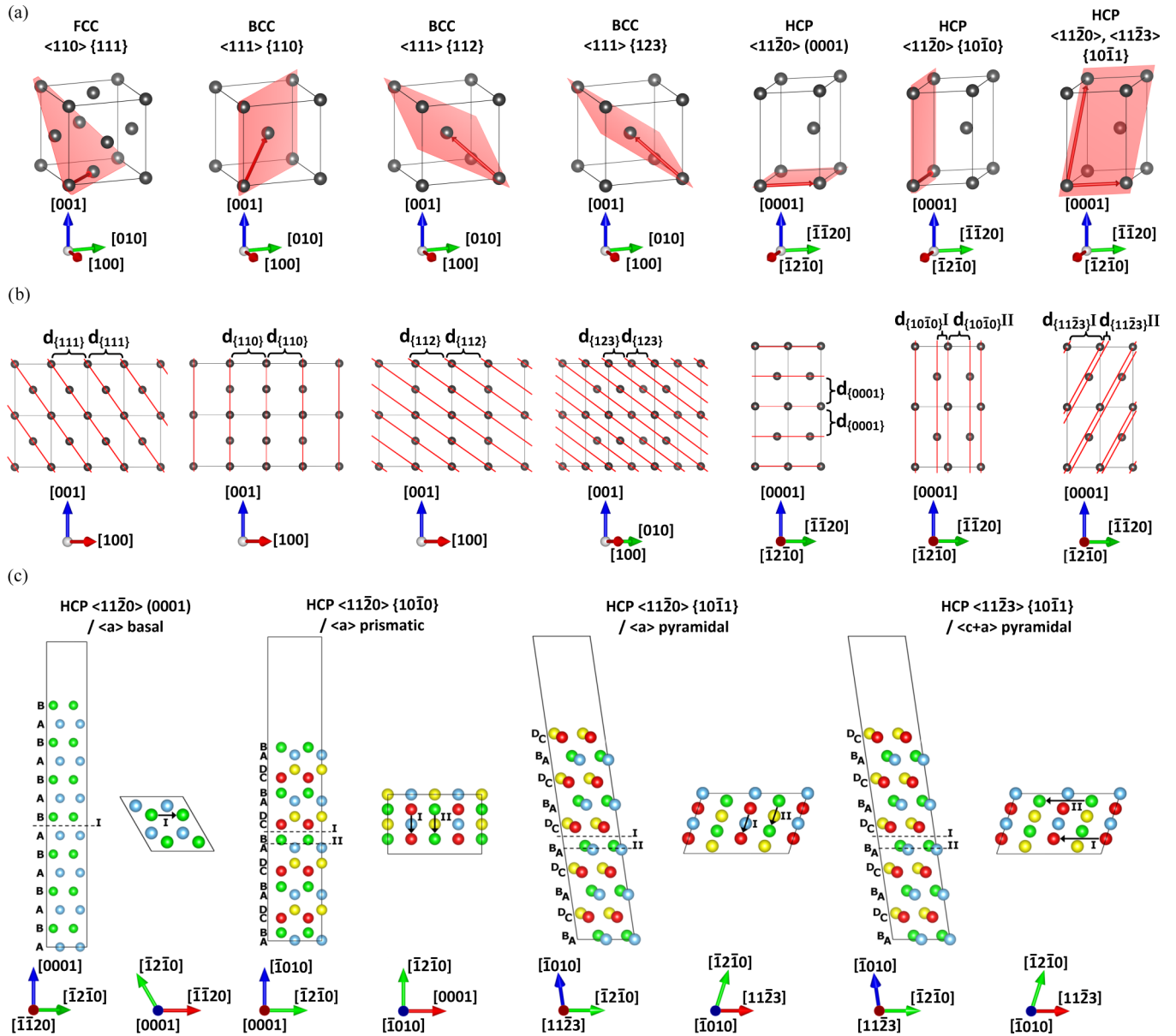


FIG. 1. (Color online) (a) Slip modes in fcc, bcc, and hcp single unit cells. The Burgers vectors and glide planes are labeled as red vectors and planes, respectively. (b) The interplanar spacing $d_{(x)}$ is shown in the side view (parallel to the glide planes) of the $2 \times 2 \times 2$ unit cells. (c) The slab supercells used in γ curve calculations; arrows marked I and II describe split slip modes with different interplanar distance, while A,B,C,D denote the stacking sequence of atomic planes (colored spheres).

planes and vacuum region should be big enough to prevent interaction between the free surfaces and slip planes. Further increases in the size of atomic planes did not improve the quality of the γ results. The relaxation of ions was stopped when 1 and 30 meV/Å force (for equilibrium and distorted structures, respectively) and 1 meV energy convergences were reached. These parameters allowed one to obtain very good agreement of lattice constants $a = 2.94$ Å and $c/a = 1.583$ with experiments $a = 2.95$ Å and $c/a = 1.587$ [26]. In the second part of our calculations, we used the climbing image-nudged elastic band (CI-NEB) method [27] to determine the γ curves along the unconstrained path (nine transition images) of crystal slips with precise values of saddle points— $\gamma_{(NEB)us}$. In order to achieve the listed force and energy convergence

criteria, global force NEB optimizations (instead of image by image) were performed using limited-memory Broyden-Fletcher-Goldfarb-Shanno, fast inertial relaxation engine and quick-min ionic optimizers [28].

IV. RESULTS AND DISCUSSION

The results of conventional rigid γ curve computations for straight slip paths are shown in Fig. 2(a) as dotted lines. It should be noted that the differences between the type-I and type-II split modes are significant. Unique are $\langle a \rangle$ pyramidal modes with smaller γ_{us} for type II, which is the inverse to the Peierls relation [Eq. (2)] that predicts lower Peierls stress for longer interplanar distances. Nevertheless, the rigid

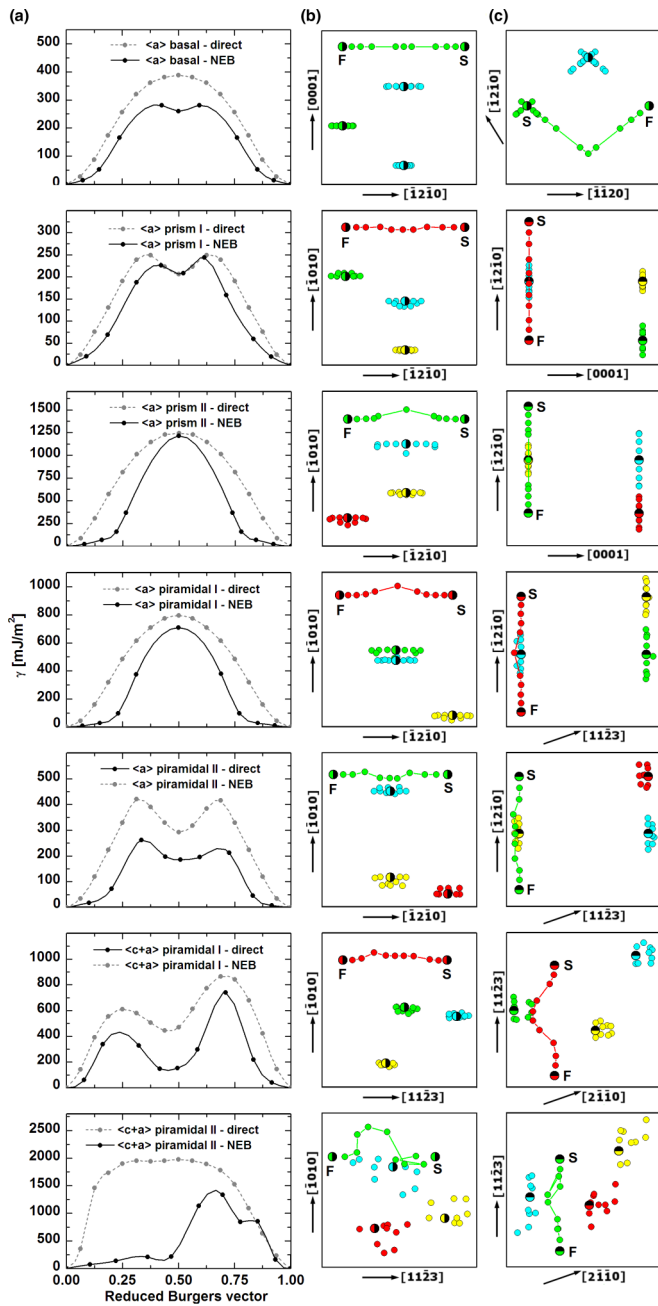


FIG. 2. (Color online) (a) Results of the rigid (direct) and NEB γ curve calculations for seven α -Ti slip modes, slip traces (solid colored lines), and movements of atoms [colored circle stacking is similar to Fig. 1(c)] located below the glide planes: (b) view perpendicular to Burgers vector and parallel to glide plane, and (c) view perpendicular to Burgers vector and glide plane. The half black points represent equilibrium positions, and “S” and “F” symbols indicate start and finish of the slip paths, respectively.

γ results contain a few failures. Apart from the absence of elastic deformation correction, the path of crystal slips can be nonstraight [colored lines in Fig. 2(c)]. When analyzing the geometries of slip planes [Fig. 1(c)], it can be seen that in the basal mode, the glide should be executed according to the dissociation of dislocations mechanism. A similar manner is expected in $\langle c+a \rangle$ pyramidal modes in which atoms adjacent

to the glide planes (red/green atoms for type I and green/blue for type II) repel each other during slip. Calculation of the full γ surfaces cannot fix these problems since the minimum-energy path (MEP) determined in this way would still be burdened by the rigid model regime.

An excellent opportunity to resolve all issues regarding the rigid γ is to be found in the nudged elastic-band method (NEB) [28,29]. The NEB is an MEP finding tool for transitions between known initial and final states. The great advantage of the NEB is the possibility to perform all-dimension relaxations of metastable systems. The importance of atomic relaxation in the context of Peierls stress has been reported in the past [30], with the conclusion being that atomic displacements are crucial for accurate lattice resistance results. Furthermore, NEB has also been employed to predict the mobility of screw dislocations in silicon [31]. The results of computed $\gamma_{(NEB)}$ curves (solid lines) together with slip traces and movements of atoms located below glide planes are shown in Fig. 2. All of the obtained $\gamma_{(NEB)}$ wave forms exhibit pronounced differences to the rigid γ curves, which are the results of two effects. The first is the contribution of elastic deformation energy, leading to a reduction in γ values at the beginning and end of the slips. The elastic shifts of atoms below the slip planes are significant, with displacement amplitude reaching half the value of the Burgers vector [$\langle a \rangle$ prism II and $\langle a \rangle$ pyramidal I in Figs. 2(b) and 2(c)]. In addition, the size of these movements increases with $\gamma_{(NEB)us}$ values, which appears to be physically reasonable. The second factor affecting the γ curves is the shape of the slip trace. Of all the modes, only slip along prism planes runs straight, causing similar $\gamma_{(NEB)us}$ and γ_{us} results (Table I). The nonstraight NEB paths [colored lines in Fig. 2(c) for all pyramidal modes] of the slips depend on crystal geometry and enable serious reduction of γ_{us} values. However, it should be emphasized that nonstraight slip trace and elastic effects are mutually linked. An initial elastic deformation changes atomic positions below and above the glide planes, which results in different interplanar potential than occurs in the rigid γ model and enables one to determine the authentic, lowest-energy, splinelike slip tracks. This fact allows one to obtain a dissociated wave form of the slip in basal mode and the curved slip trace in pyramidal systems, as seen in Fig. 2(c). The NEB calculations also confirm the existence of inverse Peierls relations [Eq. (2)] for $\langle a \rangle$ pyramidal systems. As is shown in Fig. 3, in the middle of the type-I slip, pairs of atomic planes adjacent to the glide plane are directly above each other, generating a strong energy barrier which does not appear in $\langle a \rangle$ pyramidal II mode. This explains the higher value of $\gamma_{(NEB)us}$ in the type-I system.

Since the unstable stacking fault energies cannot be measured experimentally, the results of γ computations have been evaluated through comparison of the calculated values of maximum restoring stresses F [Eq. (1)] with experimental CRSS, which define the shear stresses component required to initiate slip in a grain. As the compared quantities are not physically equal, their normalized values are listed in Table I.

The comparison of F_{max} , $F_{(NEB)max}$, and CRSS ratios shows that the NEB method allows for a significantly better projection of deformation by the slip mechanism than the standard γ approach. It can be seen that the critical restoring forces calculated from γ -NEB curves can be efficiently used

TABLE I. Comparison of calculated unstable stacking fault results, their ratios, and proportions of experimental CRSS values. The γ and F_{\max} values are in mJ/m^2 and $\text{meV}/\text{\AA}^3$, respectively.

(X)	Slip system	γ_{us}	$\gamma_{(\text{NEB})\text{us}}$	F_{\max}	$F_{(\text{NEB})\text{max}}$	$\frac{F_{\max(X)}}{F_{\max(1)}}$	$\frac{F_{(\text{NEB})\text{max}(X)}}{F_{(\text{NEB})\text{max}(1)}}$	$\frac{\text{CRSS}(X)}{\text{CRSS}(1)}$
1	$\langle a \rangle$ prism I	249	244	20.52	20.83	1.00	1.00	1.00^{a,b}
2	$\langle a \rangle$ prism II	1243	1215	91.22	95.38	4.44	4.58	
3	$\langle a \rangle$ basal	388	280	29.25	22.88	1.43	1.10	1.19^a, 1.15^b
4	$\langle a \rangle$ pyram. I	796	708	56.16	68.38	2.74	3.28	
5	$\langle a \rangle$ pyram. II	421	261	35.76	25.61	1.74	1.23	1.08^a
6	$\langle c + a \rangle$ pyram. I	864	740	45.36	49.21	2.21	2.36	2.62^b
7	$\langle c + a \rangle$ pyram. II	1977	1334	201.10	48.83	9.80	2.34	

^aExperimental values from Ref. [18].

^bIn Ref. [17], the CRSS values were determined via the reverse process of fitting the model load-displacement curves to experimental ones.

for a qualitative description of individual slip modes. The values of γ_{us} , and F_{\max} for both rigid and NEB approaches, are significantly lower for systems with greater interplanar spacing, except for the $\langle a \rangle$ pyramidal II mode, implying that the distance between glide planes and the atomic configuration during the slip has a dominant impact on these parameters. The γ_{us} , $\gamma_{(\text{NEB})\text{us}}$, F_{\max} , and $F_{(\text{NEB})\text{max}}$ are also similar for the lower-energy modes with the same Burgers vector length $\langle a \rangle$ and are much higher for longer $\langle c + a \rangle$ slip vectors, which agrees well with experiments [17,18]. The elastic displacements of atomic positions together with nonstraight slip paths [Figs. 2(b) and 2(c)] cause a pronounced reduction of $\gamma_{(\text{NEB})\text{us}}$ relative to γ_{us} in most systems. The results in Table I denote four active α -Ti slip systems which, in ascending order, are $\langle a \rangle$ prism I, $\langle a \rangle$ pyramidal II, $\langle a \rangle$ basal, and $\langle c + a \rangle$ pyramidal I [smaller $\gamma_{(\text{NEB})\text{us}}$]. Although the sequence of planes was already known, the partition in terms of split modes is additionally described here. The other three split systems ($\langle a \rangle$ prism II, $\langle a \rangle$ pyramidal I, and $\langle c + a \rangle$ pyramidal II) are inactive because the slip can always be realized along an easier adjacent mode. The calculated transition atomic structures indicate that

the nucleation of dislocations is fully performed in individual active systems without any dividing of the crystal slip into parallel planes. There is no physical reason for distributed slip along two glide planes with distinctly different γ_{us} and F_{\max} . Even if the crystal slip could occur simultaneously in both split modes, it would be visible in atomic positions presented in Fig. 2. However, it is not. This demonstrates that the split phenomenon concerns only slip modes, not slip of the dislocations—it reveals the existence of hcp prismatic and pyramidal submodes with various interplanar distance, and executed calculations define modes in which dislocations can nucleate and move.

V. CONCLUSIONS

In summary, this paper presents a computational approach, based on the NEB method, to overcome the rigid γ model. This approach takes into account elastic deformation and indirect slip shape during γ curve computations, improving the overall accuracy of the energetics of crystal slips. The split slip modes phenomenon, fundamental to hexagonal crystals in plastic deformation physics, is also demonstrated here with the conclusion that the standard definition of slip systems should be expanded to include an interplanar distance expression for a precise description of prism and pyramidal modes. The results obtained agree very well with experimental data and clearly show active deformation modes in α -Ti. These allow one to indicate the unique $\langle a \rangle$ pyramidal II system, which shows that the Peierls relation is not applicable in split hexagonal modes.

The presented calculation methodology in combination with the determined active hcp slip systems can be used as an effective tool for the prediction role of the individual slip modes in the alloying of hexagonal structures. Such a broad-based approach will be highly valuable when designing new light, strong materials.

ACKNOWLEDGMENTS

This work was supported by the Polish National Centre for Research and Development under Grant No. IN1/31/158446/NCBR/12. Computing resources were provided by HPC facilities of the Interdisciplinary Centre for Mathematical and Computational Modelling at Warsaw University.

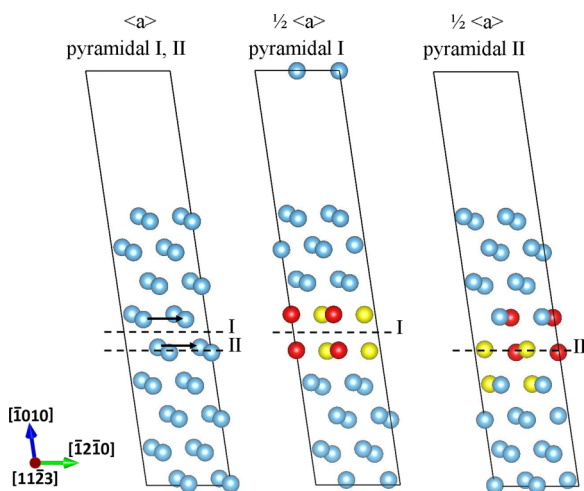


FIG. 3. (Color online) The $\langle a \rangle$ pyramidal slip modes with marked different interplanar spacing (dashed lines). The arrows denote Burgers vector and the pairs of red and yellow spheres [the colors are not equivalent to those used in Fig. 1(c)] indicate the position of the atomic planes above and below the glide plane in the middle of the slip. The presented structures were calculated with NEB.

- [1] C. Ravi, P. Vajeeston, S. Mathijaya, and R. Asokamani, *Phys. Rev. B* **60**, 15683 (1999).
- [2] S. Pugh, *Philos. Mag.* **45**, 823 (1954).
- [3] R. Peierls, *Proc. Phys. Soc.* **52**, 34 (1940).
- [4] F. R. N. Nabarro, *Proc. Phys. Soc.* **59**, 256 (1947).
- [5] J. W. Christian and V. Vitek, *Rep. Prog. Phys.* **33**, 307 (1970).
- [6] B. Joós, Q. Ren, and M. S. Duesbery, *Phys. Rev. B* **50**, 5890 (1994).
- [7] B. Joós and M. S. Duesbery, *Phys. Rev. Lett.* **78**, 266 (1997).
- [8] V. V. Bulatov and E. Kaxiras, *Phys. Rev. Lett.* **78**, 4221 (1997).
- [9] G. Lu, N. Kioussis, V. V. Bulatov, and E. Kaxiras, *Phys. Rev. B* **62**, 3099 (2000).
- [10] J. R. Rice and R. Thomson, *Philos. Mag.* **29**, 73 (1974).
- [11] J. R. Rice, *Topics in Fracture and Fatigue*, edited by A. S. Argon (Springer-Verlag, Berlin, 1992); *J. Mech. Phys. Solids* **40**, 239 (1992).
- [12] E. Tadmor and S. Hai, *J. Mech. Phys. Solids* **51**, 765 (2003).
- [13] U. Waghmare, E. Kaxiras, and M. Duesbery, *Phys. Status Solidi B* **217**, 545 (2000).
- [14] J. Hirth and J. Lothe, *Theory of Dislocation*, 2nd ed. (Wiley, New York, 1992).
- [15] S. Yip, *Handbook of Materials Modelling* (Springer, New York, 2005), pp. 793–811.
- [16] D. Hull and D. Bacon, *Introduction to Dislocations*, 4th ed. (Butterworth-Heinemann, Oxford, 2001).
- [17] J. Gong and A. J. Wilkinson, *Acta Mater.* **57**, 5693 (2009).
- [18] A. T. Churchman, *Proc. Roy. Soc. A* **226**, 216 (1954).
- [19] S. Zaeferrer, *Mater. Sci. Eng. A* **344**, 20 (2003).
- [20] A. Poty, J.-M. Raulot, H. Xu, J. Bai, C. Schuman, J.-S. Lecomte, M.-J. Philippe, and C. Esling, *J. App. Phys.* **110**, 014905 (2011).
- [21] G. Kresse and J. Hafner, *Phys. Rev. B* **47**, 558 (1993).
- [22] G. Kresse and J. Furthmüller, *Phys. Rev. B* **54**, 11169 (1996).
- [23] P. E. Blöchl, *Phys. Rev. B* **50**, 17953 (1994).
- [24] J. P. Perdew, K. Burke, and M. Ernzerhof, *Phys. Rev. Lett.* **77**, 3865 (1996); **78**, 1396(E) (1997).
- [25] H. J. Monkhorst and J. D. Pack, *Phys. Rev. B* **13**, 5188 (1976).
- [26] G. Lutjering and J. Williams, *Titanium* (Springer-Verlag, Berlin, 2003).
- [27] G. Henkelman, B. P. Uberuaga, and H. Jónsson, *J. Chem. Phys.* **113**, 9901 (2000).
- [28] D. Sheppard, R. Terrell, and G. Henkelman, *J. Chem. Phys.* **128**, 134106 (2008).
- [29] D. Sheppard and G. Henkelman, *J. Comput. Chem.* **32**, 1769 (2011).
- [30] G. Lu, N. Kioussis, V. V. Bulatov, and E. Kaxiras, *Philos. Mag. Lett.* **80**, 675 (2000).
- [31] L. Pizzagalli, P. Beauchamp, and H. Jónsson, *Philos. Mag.* **88**, 91 (2008).